Synthesis and crystal structure of double-perovskite compound Sr_2FeMoO_6

Y. C. Hu, J. J. Ge, Q. Ji, B. Lv, and X. S. Wu[a)]
Nanjing National Laboratory of Microstructures, Key Lab of Solid State Microstructures and Department of Physics, Nanjing University, Nanjing 210093, China

G. F. Cheng
Shanghai Institute of Ceramics, Chinese Academy of Sciences, 1295 Dingxi Road, Shanghai 200050, China

(Received 1 February 2010; accepted 3 June 2010)

Samples of single-phase Sr_2FeMoO_6 were successfully prepared by solid-state reaction with long sintering times. The crystal structures of the Sr_2FeMoO_6 samples were determined from X-ray powder diffraction data using the Rietveld refinement method. The structure results obtained by the Rietveld refinements show that an increase in the total sintering time of the solid-state reaction is an effective method to obtain single Sr_2FeMoO_6 phase and to improve the ordering of Fe and Mo cations (or reducing antisite defects) in the double-perovskite structure. The volume of the tetragonal unit cell of Sr_2FeMoO_6 contracts slightly after successive sintering treatments. The averaged Fe-O and Mo-O bond lengths as well as the tilt between the FeO_6 and the MoO_6 octahedra decrease with increasing total sintering time. Our results suggest that the detected subtle changes in crystal structure, such as bond lengths and bond angles between the Fe and Mo cations and oxygen, in the ordered double-perovskite structure may be responsible for the large effects on previously reported transport and magnetic properties of an oxide metal. © *2010 International Centre for Diffraction Data.* [DOI: 10.1154/1.3478711]

Key words: X-ray diffraction, synthesis process, crystal structure, Sr_2FeMoO_6

I. INTRODUCTION

Double perovskite compounds including Sr_2FeMoO_6 (SFMO) are known to exhibit large magnetoresistances in weak magnetic fields (Kobayashi *et al.*, 1998). The novel magnetoresistance properties have been explained by the intergrain spin-dependent carrier scattering process. SFMO has become one of the most promising candidates in magnetic storage materials (Prinz, 1999). SFMO has a typical ordered double-perovskite structure $A_2BB'O_6$, where A is an alkali-earth ion and B and B' are transition metals. In the structure of SFMO, alternating FeO_6 and MoO_6 octahedra are arranged regularly in a rocksalt superlattice with the Sr cations occupying the voids among the octahedra. The charge and radius differences between Fe^{3+} and Mo^{5+} are 2 and 0.035, respectively, which make fractions of Fe^{3+} and Mo^{5+} occupy the B and B' sites randomly. There is also a fraction of Mo atoms located at the B site and an equivalent of Fe atoms located at the B' site, and this is known as the antisite (AS) defect. It is also well known that the AS defect strongly depends on the synthesis process (Stoeffler and Silviu, 2006). The AS defect was reported to decrease the magnetic moment of SFMO and has a large influence on its structure and magnetic properties (Navarro *et al.*, 2001). The successive sintering treatments can improve the ordering of the cations and physical properties of SFMO (Jurca *et al.*, 2009). In this paper, the results on the study of crystal structures of SFMO samples prepared by solid-state reaction with long sintering times are reported.

[a)]Author to whom correspondence should be addressed. Electronic mail: xswu@nju.edu.cn

II. EXPERIMENTAL

Sample of Sr_2FeMoO_6 was prepared by standard solid-state reaction. Stoichiometric amounts of powders of $SrCO_3$, Fe_2O_3, and MoO_3 were mixed, ground, and heated at 900 °C for 10 h in air. A small amount of the presintered sample was kept for X-ray powder diffraction (XRD) analysis and the rest of the sample was finely ground, pressed into pellets, and then sintered at 1280 °C in a stream of 5% H_2/Ar gas for 5 h. The heating and cooling rates for the sintering process at 1280 °C were 5 °C/min. One pellet was kept for XRD analysis (sample 1) and the remaining pellets were then subjected through the process of regrinding and resintering for one, two, three, and four times to produce samples 2, 3, 4, and 5, respectively. Therefore, the total sintering times (at 900 and 1280 °C) used to synthesize samples 1, 2, 3, 4, and 5 were 5, 10, 15, 20, and 25 h, respectively.

Crystalline phases and crystal structures of the samples were studied by XRD using a Rigaku D/max 2500 diffractometer. The diffraction data were collected at room temperature (300 K) over a 2θ range of 20° to 100°. Other experimental conditions were diffracted-beam graphite monochromator, Cu $K\alpha$ radiation, 45 kV, 120 mA, and θ-2θ scan with 2θ steps of 0.02° and count time per step of 2 s. The Rietveld refinement program GSAS (Toby, 2001) was used for crystal-structure determination from the experimental XRD data.

III. RESULTS AND DISCUSSION

A. Crystalline phase

The XRD pattern for the presintered sample is shown in Figure 1. In the presintered process, the main reactions can be described by the following equations:

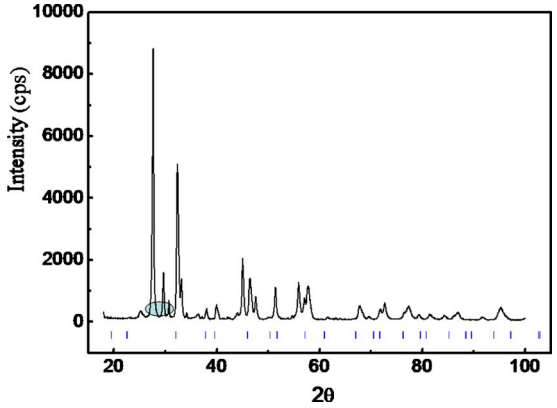

Figure 1. (Color online) XRD pattern for the presintered sample prepared at 900 °C for 10 h in air. The three peaks appeared in the 2θ range indicated by the oval are the main peaks of $SrMoO_4$. The vertical bars at the bottom indicate the Bragg reflection positions for Sr_2FeMoO_6.

$$SrCo_3 \xrightarrow{900\ ^\circ C} SrO + CO_2\uparrow, \quad (1)$$

$$8SrO + 2Fe_2O_3 + 4MoO_3 \rightarrow 4Sr_2FeMoO_6 + O_2\uparrow, \quad (2)$$

$$SrO + MoO_3 \xrightarrow{O_2} SrMoO_4. \quad (3)$$

The electronic configuration of Mo is $4d^55s^1$ and the stable valance of Mo is +6. The reaction of Eq. (3) is more prone to occur in the presintered process. This can be seen from Figure 1, in which the three peaks appeared in the 2θ range indicated by the oval are the main peaks of $SrMoO_4$. According to the results of the Mossbauer spectrum obtained by Lindén *et al.* (2004), the main valences of Fe and Mo cations in SFMO are +3 and +5, respectively. Thus, the presintered mixture needs to process further in reducing atmosphere in order to reduce Mo^{+6} in $SrMoO_4$ to Mo^{+5} in SFMO. The reducing atmosphere of 5% to 95% H_2/Ar was used based on the results of our previous study (Hu *et al.*, 2009) that the reducing atmosphere of 5 to 95% H_2/Ar can effectively reduce Mo^{6+} to Mo^{5+} and prevent the reduction of Fe^{3+} to Fe. Figure 2 shows the XRD pattern for sample 1, and the two peaks appeared in the 2θ range indicated by the oval are the main peaks of $SrMoO_4$ with significantly smaller intensities than those of the prereacted mixture shown in Figure 1. Therefore, the amount of $SrMoO_4$ in sample 1 is significantly smaller than that in the presintered sample. Figure 3 shows the XRD pattern for sample 2 with only about 2% of $SrMoO_4$. Figure 4 shows XRD pattern for sample 3 with a total sintering time of 15 h, and it can clearly be seen that sample 3 is pure Sr_2FeMoO_6, and no trace of $SrMoO_4$ can be detected. The total chemical reaction equation for synthesizing a pure SFMO phase is as follows:

$$8SrCo_3 + 2Fe_2O_3 + 4MoO_3 \rightarrow 4Sr_2FeMoO_6 + O_2\uparrow + 8CO_2\uparrow.$$

The XRD patterns for samples 4 and 5 are similar to that of sample 3 shown in Figure 3, showing that only the SFMO phase is presented in samples 3 and 4.

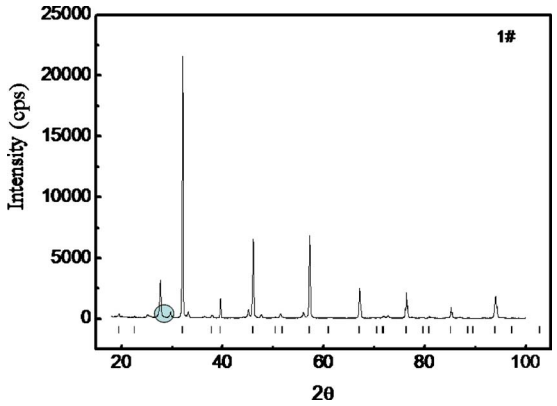

Figure 2. (Color online) XRD pattern for sample 1. The two peaks appeared in the 2θ range indicated by the oval are the main peaks of $SrMoO_4$. The vertical bars at the bottom indicate the Bragg reflection positions for Sr_2FeMoO_6.

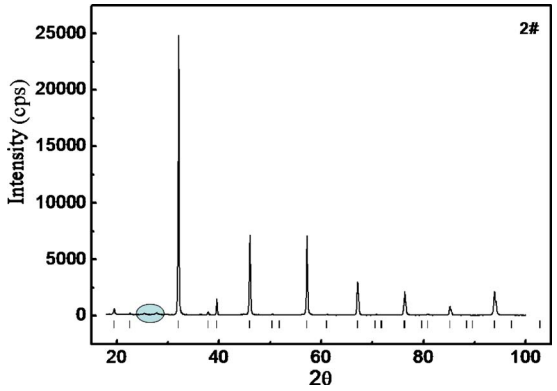

Figure 3. (Color online) XRD pattern for sample 2. The two peaks appeared in the 2θ range indicated by the oval are the main peaks of $SrMoO_4$. The vertical bars at the bottom indicate the Bragg reflection positions for Sr_2FeMoO_6.

B. Crystal structure

The Rietveld refinements of X-ray diffraction patterns of SFMO for samples 3, 4, and 5 were carried out based on a tetragonal structure with space group $I4/m$ and Sr located at the 4*d* site of (1/2, 0, 1/4), Fe/Mo at both the *B* site of 2*a* (0, 0, 0) and the *B′* site of 2*b* (0, 0, 1/2), and O1 at 8*h* (*x*, *y*, 0) and O2 at 4*e* (0, 0, *z*). Before each refinement, we assume full occupancy for each site. In addition, the sum of the oc-

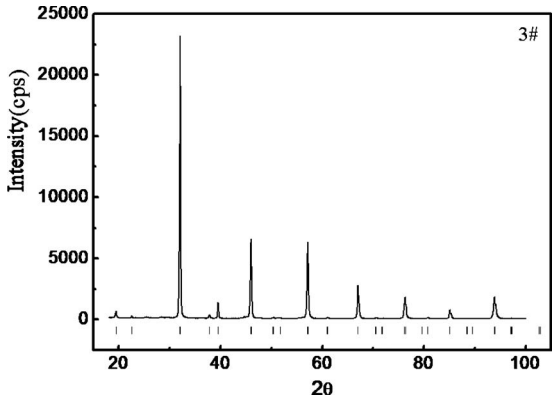

Figure 4. XRD pattern for sample 3. The vertical bars at the bottom indicate the Bragg reflection positions for Sr_2FeMoO_6. Similar XRD patterns were obtained for samples 4 and 5.

https://doi.org/10.1154/1.3478711 Published online by Cambridge University Press

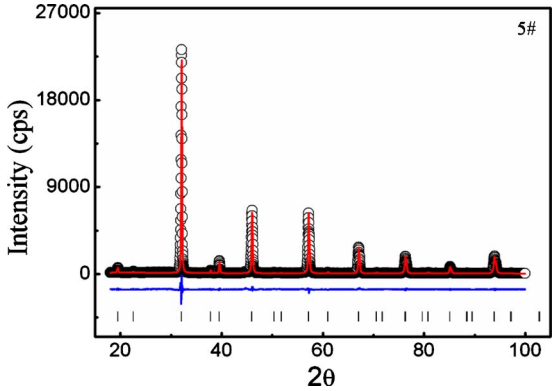

Figure 5. (Color online) Observed (circles) and calculated (continuous line) XRD patterns for sample 5. The vertical bars at the bottom indicate the Bragg reflection positions for Sr_2FeMoO_6. The lowest curve shows the differences between the observed and the calculated XRD patterns.

cupancies of the Fe cations at both the B and the B' sites was also fixed to 1.0, the same for the Mo cations. The reason for assuming full oxygen occupancies at the O1 and the O2 sites was the uncertainty caused by weak X-ray scattering by oxygen (Wu *et al.*, 1998). Each refinement was performed according to the refinement order previously reported by Wu *et al.* (1996). Figure 5 shows the refinement results on sample 5, and similar crystal-structure results were obtained for samples 3 and 4. Refined crystal-structure parameters and R factors for samples 3, 4, and 5 are listed in Table I, and values of bond lengths and bond angles of the three samples are also listed in Table II.

As shown in Table I, the values of a, c, a/c, and V decrease systematically with increasing sintering time. The occupancy of Fe at the B site increases with increasing sintering time. By defining the degree of ordering of the Fe or Mo cation to be $\eta=1-2\mathrm{AS}$, where AS represents the antisite occupancy, the value of η increases almost linearly from 44.9(2)% for sample 3 to 80.2(4)% for sample 5. This indicates that the increases in the sintering time did improve the ordering of cations (or reduce the number of antisite defects) in SFMO.

TABLE II. Bond lengths and angles for samples 3, 4, and 5 of Sr_2FeMoO_6 obtained by the Rietveld refinements.

Bond lengths	Sample 3	Sample 4	Sample 5
Sr-O(1)×4 Å	2.798 63(4)	2.798 00(2)	2.797 38(4)
Sr-O(1)×4 Å	3.146 52(1)	3.128 75(4)	3.067 98(3)
Sr-O(2)×4 Å	2.791 65(4)	2.790 79(2)	2.789 75(5)
Fe-O(1)×4 Å	2.202 94(3)	2.202 26(2)	2.201 44(4)
Fe-O(2)×2 Å	1.986 40(4)	1.986 11(2)	1.985 98(4)
Averaged Fe-O	2.130 76(3)	2.130 21(2)	2.129 62(4)
Δ_1	0.216 53(9)	0.216 15(0)	0.215 45(9)
O2-Fe1-O1 (deg)	90	90	90
Mo-O(1)×4 Å	1.744 98(3)	1.744 44(2)	1.743 79(3)
Mo-O(2)×2 Å	1.954 87(4)	1.954 58(2)	1.954 45(5)
Averaged Mo-O	1.814 94(7)	1.814 48(9)	1.814 01(3)
Δ_2	0.209 89(1)	0.210 14(0)	0.210 66(2)
O2-Mo1-O1 (deg)	90	90	90
Fe-O(1)-Mo (deg)	171.9(3)	172.8(4)	174.2(6)
Fe-O(2)-Mo (deg)	180.000(0)	180.000(0)	180.000(0)

Table II shows the values of bond lengths and angles for SFMO samples 3, 4, and 5 prepared by total sintering times of 15, 20, and 25 h, respectively. As shown in Table II, the average Fe-O and Mo-O bond lengths decrease with increasing sintering time. The value of Δ_1 (where $\Delta_1=|l_{\mathrm{Fe\text{-}O(1)}}-l_{\mathrm{Fe\text{-}O(2)}}|$ and $l_{\mathrm{Fe\text{-}O(1)}}$ and $l_{\mathrm{Fe\text{-}O(2)}}$ are the bond lengths of Fe-O1 and Fe-O2, respectively) decreases with increasing sintering time, indicating that the difference between the lengths of the Fe-O1 and Fe-O2 bonds is getting smaller. On the other hand, the value of Δ_2 (where $\Delta_2=|l_{\mathrm{Mo\text{-}O(1)}}-l_{\mathrm{Mo\text{-}O(2)}}|$ and $l_{\mathrm{Mo\text{-}O(1)}}$ and $l_{\mathrm{Mo\text{-}O(2)}}$ are the bond lengths of Mo-O1 and Mo-O2, respectively) increases with increasing sintering time, indicating that the difference between the lengths of the Mo-O1 and Mo-O2 bonds is becoming larger.

TABLE I. Crystal-structure parameters, site occupancies, and degrees of Fe and Mo orderings, η, obtained by the Rietveld refinements of XRD patterns of samples 3, 4, and 5 of Sr_2FeMoO_6.

		Sample 3	Sample 4	Sample 5
a (Å)		5.583 20(5)	5.581 48(4)	5.579 40(4)
c (Å)		7.882 53(4)	7.881 37(8)	7.880 85(6)
a/c		0.708 30(1)	0.708 18(6)	0.707 96(9)
V (Å^3)		245.71(6)	245.52(8)	245.32(9)
Fe1	2a (0 0 0) occupancy	0.724(6)	0.813(5)	0.901(2)
Fe2	2b (0 0 1/2) occupancy	0.275(4)	0.186(5)	0.098(8)
Mo1	2b (0 0 1/2) occupancy	0.724(6)	0.813(5)	0.901(2)
Mo2	2a (0 0 0) occupancy	0.275(4)	0.186(5)	0.098(8)
η (%)		44.9(2)	62.7(0)	80.2(4)
O1	8h (x y 0)			
	x	0.279 00(1)	0.281 02(4)	0.283 21(6)
	y	0.265 00(2)	0.262 04(5)	0.261 78(2)
O2	4e (0 0 z)			
	z	0.252 00(2)	0.250 11(2)	0.249 30(1)
R_{wp} (%)		10.41	9.28	9.92
R_p (%)		7.59	6.86	6.76
R_{exp} (%)		6.75	5.41	5.12

https://doi.org/10.1154/1.3478711 Published online by Cambridge University Press

TABLE III. X-ray diffraction data for sample 5 of Sr_2FeMoO_6.

$2\theta_{cal}$ (deg)	I_{cal} (counts/s)	I_{obs} (counts/s)	*h k l*	$2\theta_{cal}$ (deg)	I_{cal} (counts/s)	I_{obs} (counts/s)	*h k l*	$2\theta_{cal}$ (deg)	I_{cal} (counts/s)	I_{obs} (counts/s)	*h k l*
19.477	658	593	0 1 1	67.084	2775	2768	2 2 4	88.461	110	105	2 3 5
22.517	260	236	1 1 0	70.555	128	152	4 1 1	88.461	110	105	3 2 5
22.545	275	240	0 0 2	70.555	128	152	1 4 1	88.525	70	83	0 1 7
32.056	20 253	19 441	0 2 0	70.577	133	157	3 2 3	89.487	65	81	5 1 0
32.076	22 660	21 172	1 1 2	70.577	133	157	2 33	89.487	65	81	1 5 0
37.785	346	339	2 1 1	70.622	156	157	1 2 5	89.529	68	84	3 3 4
37.785	346	339	1 2 1	70.622	156	157	2 1 5	89.583	60	84	2 2 6
37.820	380	381	0 1 3	71.706	90	96	3 3 0	93.868	1682	1633	5 1 2
39.546	1211	1201	0 2 2	71.717	88	98	0 4 2	93.868	1682	1633	1 5 2
45.968	5078	5103	2 2 0	71.751	101	99	3 1 4	93.900	1828	1796	4 2 4
46.027	6562	6354	0 0 4	71.751	101	99	1 3 4	93.900	1828	1796	2 4 4
50.369	173	131	0 3 1	71.807	103	97	0 0 6	93.954	1755	1764	3 1 6
50.397	186	142	2 1 3	76.251	1487	1575	4 2 0	93.954	1755	1764	1 3 6
50.397	186	142	1 2 3	76.251	1487	1575	2 4 0	97.152	101	90	5 2 1
51.769	124	119	3 1 0	76.262	1683	1680	3 3 2	97.152	101	90	2 5 1
51.769	124	119	1 3 0	76.35	1794	1785	1 1 6	97.173	97	91	4 3 3
51.783	133	123	2 2 2	79.626	91	90	4 1 3	97.173	97	91	0 5 3
51.823	138	125	1 1 4	79.626	91	90	1 4 3	97.173	97	91	3 4 3
57.152	5938	6002	3 1 2	79.670	102	90	0 3 5	97.216	94	93	4 1 5
57.152	5938	6002	1 3 2	80.721	149	149	4 2 2	97.216	94	93	1 4 5
57.190	6314	6258	0 2 4	80.721	149	149	2 4 2	97.281	88	91	1 2 7
60.963	167	181	3 2 1	80.807	166	162	0 2 6	97.281	88	91	2 1 7
60.963	167	181	2 3 1	85.156	89	93	0 4 4	102.694			4 4 0
60.987	127	188	0 3 3	88.397	63	76	0 5 1	102.869			0 0 8
61.036	147	193	0 1 5	88.397	63	76	4 3 1	106.101			5 2 3
67.037	2458	2454	0 4 0	88.397	63	76	3 4 1	106.215			0 3 7

The angles for O2-Fe1-O1 and O2-Mo1-O1 remain constant at 90°, and the angles for Fe-O2-Mo are also unchanged at 180°. However, the angle for Fe-O1-Mo increases from 171.9° to 174.2° with increasing total sintering time from 15 to 25 h. The angle for Fe-O1-Mo gradually moves closer to 180° with increase sintering time indicating that the connected Fe-O1 and O1-Mo bonds align toward a straight line as that for Fe-O2-Mo. This suggests that the tilt between the neighboring FeO_6 and the MoO_6 octahedra becomes smaller with larger sintering time, and this structural change may have an effect on the exchange interactions among Fe-O-Fe and Mo-O-Mo. The calculated XRD data for sample 5 are listed in Table III.

IV. CONCLUSION

Long total sintering times of 15 and more hours at 1280 °C were found to be essential to synthesize single-phase Sr_2FeMoO_6 by solid-state reaction. The Rietveld refinement results show that the ordering of the Fe and Mo cations (or the reduction of antisite defects) in the Sr_2FeMoO_6 structure improves with increasing total sintering time. The unit-cell volume and the average Fe-O and Mo-O bond lengths decrease with increasing sintering time. The difference between the two Fe-O bond lengths in a FeO_6 octahedron also decreases with increasing sintering time. On the other hand, the difference between the two Mo-O bond lengths in a MoO_6 octahedron becomes larger with increasing sintering time. The crystal-structure results obtained by this study may provide useful information to the understanding of the mechanism of room-temperature magnetoresistance in an oxide material with an ordered double-perovskite structure previously reported by Kobayashi *et al.* (1998).

ACKNOWLEDGMENTS

This work was supported by NNSFC (Grant Nos. 10974081, 10774065, and 10523001) and NKPBRC (Grant Nos. 2006CB921802 and 2010CB923404).

Hu, Y. C., Wang, P. F., Lv, B., Ji, Q., Wu, X. S., and Lu, Q. F. (**2009**). "Positron annihilation spectroscopy and transport properties of double perovskite compound $Sr_{2-x}Gd_xFeMoO_6$," J. Appl. Phys. **105**, 07D726–07D726-3.

Jurca, B., Berthon, J., Dragoe, N., and Berthet, P. (**2009**). "Influence of successive sintering treatments on high ordered Sr_2FeMoO_6 double perovskite properties," J. Alloys Compd. **474**, 416–423.

Kobayashi, K.-I., Kimura, T., Sawada, H., Terakura, K., and Tokura, Y. (**1998**). "Room-temperature magnetoresistance in an oxide material with an ordered double-perovskite structure," Nature (London) **395**, 677–680.

Lindén, J., Shimada, T., Motohashi, T., Yamauchi, H., and Karppinen, M. (**2004**). "Iron and molybdenum valence in double-perovskite $(Sr, Nd)_2FeMoO_6$: Electron-doping effects," Solid State Commun. **129**, 129–133.

Navarro, J., Frontera, C., Balcells, L. L., Martínez, B., and Fontcuberta, J. (**2001**). "Raising the Curie temperature in Sr_2FeMoO_6 double perovskites by electron doping," Phys. Rev. B **64**, 092411-092411–4.

Prinz, G. A. (**1999**). "Magnetoelectronics applications," J. Magn. Magn. Mater. **200**, 57–68.

Stoeffler, D. and Silviu, C. (**2006**). "Ab initio study of the electronic structure of Sr_2FeMoO_6 double perovskites presenting oxygen vacancies or/and antisite imperfections," Mater. Sci. Eng., B **126**, 133–138.

Toby, B. H. (**2001**). "EXPGUI, a graphical user interface for GSAS," J. Appl. Crystallogr. **34**, 210–213.
Wu, X. S., Jiang, S. S., Lin, J., Liu, J. S., Chen, W. M., and Jin, X. (**1998**). "Microstructural variations of $YBa_2Cu_3O_y$ doped with Ca at high doping level," Physica C **309**, 25–32.
Wu, X. S., Jiang, S. S., Xu, N., Pan, F. M., Huang, X. R., Ji, W., Mao, Z. Q., Xu, G. J., and Zhang, Y. H. (**1996**). "Structure of $La_{1.85}Sr_{0.15}CuO_4$ doped with Zn in high doping level," Physica C **266**, 296–302.

https://doi.org/10.1154/1.3478711 Published online by Cambridge University Press